NUCLEAR SCIENCE AND ENGINEERING: **172**, 268–277 (2012)

Beryllium and Graphite Neutron Total Cross-Section Measurements from 0.4 to 20 MeV

M. J. Rapp,*† Y. Danon, F. J. Saglime,‡ R. M. Bahran, and D. G. Williams§

Rensselaer Polytechnic Institute
Department of Mechanical, Aerospace, and Nuclear Engineering
Troy, New York 12180-3590

and

G. Leinweber, D. P. Barry, and R. C. Block

Bechtel Marine Propulsion Corporation
Knolls Atomic Power Laboratory
P.O. Box 1072, Schenectady, New York 12301-1072

Received August 10, 2011
Accepted March 19, 2012

Abstract—*The Gaerttner Laboratory electron linear accelerator at Rensselaer Polytechnic Institute was used in the measurement of the neutron total cross section of natural beryllium and carbon (graphite) in the energy range of 0.4 to 20 MeV. Neutron transmission measurements were made using the time-of-flight method with a 100-m flight path, fast detector response and electronics, and a narrow neutron pulse width to provide good energy resolution. A method was developed to determine the time-dependent background component associated with the transmission measurement using a combination of experimental data and Monte Carlo methods. The signal-to-background ratio combined with low counting statistics error resulted in low uncertainties and highly accurate data. The graphite measurement, showing excellent agreement with the current evaluations, provided a verification of the accuracy in the measurement and analytical methods used. The measurements of beryllium resulted in an accurate measurement of total cross section, showing some deviations with commonly used evaluations and better agreement with ENDF/B-VI.8. These results can be used for the improvement of future neutron cross-section evaluations of beryllium.*

I. INTRODUCTION

Beryllium is a lightweight metal with unique physical and nuclear properties that make it useful in a variety of nuclear applications. With a low atomic number and thermal absorption cross section, beryllium has applications as both a neutron moderator and as a reflector.[1] Beryllium is also a candidate for fusion applications, with uses such as being a plasma-facing structural material as well as a neutron breeding blanket material.[2] The low density of beryllium, combined with its nuclear properties, also makes it an ideal candidate for use in space applications.[1] With such varied applications, both current and planned, precise knowledge of the total neutron cross section is required for accurate design considerations.

A review of the evaluated neutron total cross sections for beryllium displays significant differences below 1 MeV with ~8% difference below 0.6 MeV. A review of relevant experimental data from the EXFOR database[3] shows a similar variation. The goal of the present

*E-mail: rappm@rpi.edu
†Current address: Bechtel Marine Propulsion Corporation, Knolls Atomic Power Laboratory, P.O. Box 1072, Schenectady, New York 12301-1072
‡Current address: Moog Inc., East Aurora, New York 14052
§Current address: United States Military Academy, Department of Physics and Nuclear Engineering, West Point, New York 10996

work is to provide a new high-accuracy measurement of beryllium to resolve these discrepancies.

A new detector was developed at Rensselaer Polytechnic Institute (RPI) capable of collecting data in the energy range 0.4 to 20 MeV and verified using carbon as a measurement reference. The total neutron cross section of carbon is compared to previously measured data as well as the evaluated data to verify the accuracy and resolution of the system.

II. EXPERIMENTAL SETUP

Experiments were performed at the Gaerttner Linear Accelerator (LINAC) Laboratory at RPI using the high-energy modular proton recoil detector. An illustration of the experimental setup is shown in Fig. 1. Neutrons are produced using a pulsed electron beam from the linear accelerator striking water-cooled tantalum plates in the RPI neutron-producing target.[4] The neutron target described in Ref. 4 was placed on axis with the flight tube and used without moderation to maximize neutron flux in the energy region of interest.

The high-energy electrons from the linear accelerator generate bremsstrahlung X-rays within the target, which then interact with the tantalum to produce photoneutrons. These interactions produce a white neutron source, which can be approximated by an evaporation spectrum with an evaporation temperature of 0.55 MeV, with a maximum energy extending up to the maximum energy of the electron beam (~55 MeV). A more detailed analysis of the neutron flux profile can be found in Ref. 5. The collimated neutron beam is passed through a 7.62-cm-thick depleted uranium filter used to decrease the intense burst of photons (gamma flash) incident upon the detector, which otherwise would cause recovery issues with the system. This filter also eliminates any X-ray and low-energy gamma background produced in the target. The neutron beam is then further collimated to a diameter of 4.76 cm to ensure no neutrons stream around the sample material and reach the detector, which would cause excessive background counts. The beam passes through the sample materials mounted on an electronically controlled sample changer located ~13.85 m from the neutron source before continuing on to the detector located at an effective flight path of 99.95 ± 0.07 m. The flight path of the detector was determined by fitting the resonance structure seen in carbon with energies taken from ENDF/B-VII.0 (Ref. 6). The collimation system prior to the sample location combined with thick concrete shielding and the large sample-to-detector distance provide a good geometry experiment, preventing inscattering of neutrons, which would cause a source of neutron beam–dependent background. Compared to other sources of background, this component is negligible.

The detector consists of two custom-made Eljen Technology EJ-301[a] proton recoil liquid scintillator modules. While the scintillator chosen is capable of separating neutron interactions from gamma interactions by pulse shape analysis, this feature was not utilized for these measurements. The signal-to-background allowed for low statistical uncertainty without the added electronic complexity of a pulse shape analysis system. Each module is 18.3 × 35.6 × 12.7 cm deep, with two Photonis XP4572B 12.7-cm-diam photomultiplier tubes[b] to optimize light collection throughout the detector volume. The two modules stacked on top of each other give the detector system dimensions of 36.6 cm high × 35.6 cm wide normal to the neutron beam. This area was established to optimize collection of the neutron beam profile at the detector location, which was determined through calculation of

[a]http://www.eljentechnology.com/ (accessed July 20, 2010).

[b]http://www.photonis.com/industryscience/products/photomultipliers_assemblies/photomultiplier_tubes_pmt (accessed July 20, 2010).

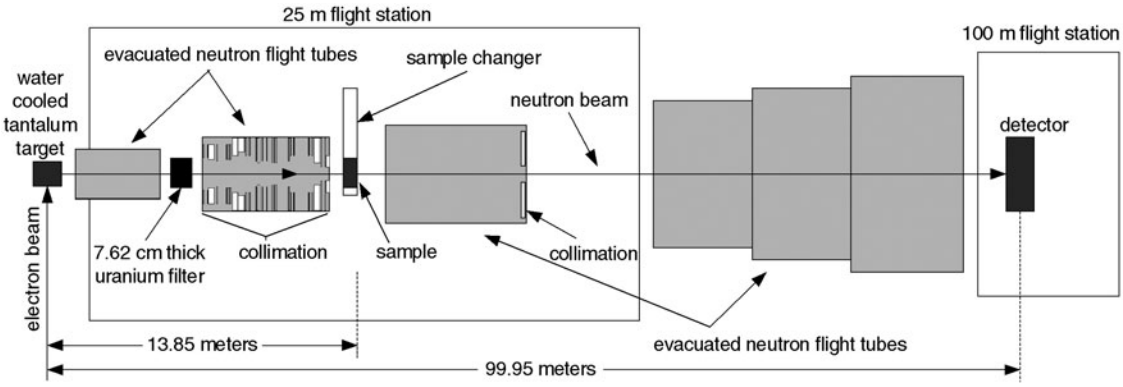

Fig. 1. Experimental setup showing the electron beam hitting the neutron-producing target, neutron collimation, flight path, and detector locations (not drawn to scale).

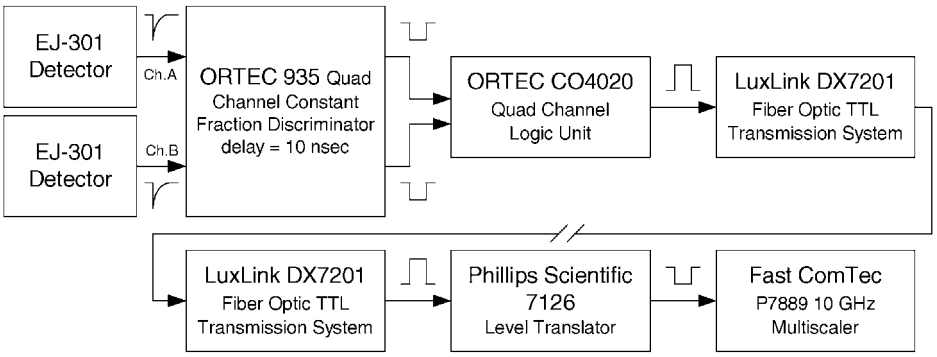

Fig. 2. Flow diagram of electronics used for data collection showing the signal path from detector to data collection at the TOF clock. The break between the two DX7201 transmission system units represents where the signal travels from the detector location at 100 m to the Gaerttner Laboratory control room where data are collected.

neutron transport through the collimation system using the MCNP5 Monte Carlo transport code[7] and verified with experimental data. The thickness of the detector was selected to maximize neutron detection efficiency while maintaining good time resolution. A 3.18-mm-thick lead shield was added around the detector to minimize the effect of low-energy gamma background.

The output from each EJ-301 module is fed to an ORTEC 935 constant fraction discriminator for optimizing time resolution over the wide range of pulse amplitudes and then summed in an ORTEC CO4020 logic unit. This output is then converted to an optical signal for transport to the data acquisition computer using a LuxLink DX7201 fiber optic TTL transmission system. The data were collected into 1.6-ns time bins using a FastComTec P7889 multiscaler board. The P7889 is a multihit time-of-flight (TOF) clock with no dead time between channels. A flow diagram of the signal can be seen in Fig. 2. The system dead time was experimentally determined to be 90 ns, which coincides with the width of the stop signal to the P7889 multiscaler. During data taking, the maximum counting rate was monitored, and the LINAC electron beam current was adjusted to maintain the dead-time correction factor below 5%.

Additional neutron detectors are installed at the LINAC facility and are used to monitor the neutron flux from the target. These monitor data are collected using two moderated fission detectors (Reuter-Stokes RS-P6-2403-121 and Amperex B300D fission chambers), which are located ~9 m from the neutron target. A third monitor is a ^{6}Li glass ring detector, which measures the penumbra of the neutron beam. The monitor data are recorded during each measurement and used to correct for variations in neutron beam intensity.

III. SAMPLES

The carbon experiment used three samples with nominal thicknesses of 7, 13, and 33 cm. The beryllium experiment used three beryllium sample thicknesses—2, 4, and 8 cm—and the 13-cm carbon sample. The carbon sample was measured during the beryllium experiment as a reference; an accurate (agreement with ENDF/B-VII.0) carbon measurement gives confidence in the beryllium measurement. Multiple thickness samples were used to optimize the sample counting statistics while minimizing the total run time as is discussed in Ref. 8. Using multiple samples also allows for comparison of the individual sample cross-section data prior to combining as a means of verification and systematic error determination. The sample diameter and weight were precisely measured to obtain the sample number density N and associated uncertainty σ_N, which can be seen in Tables I and II for the carbon experiment and beryllium experiment, respectively. Both the carbon samples and beryllium samples were analyzed to be above 99.9% purity. A more detailed description of the samples, as well as a list of impurities and associated quantities, can be obtained from Ref. 9.

IV. EXPERIMENTAL METHOD

Transmission measurements were taken using the TOF method and used to calculate the experimental neutron total cross section. The transmission for each recorded time bin is determined using Eq. (1):

$$T_i = \left[\frac{C_i^S - B_i^S}{C_i^O - B_i^O} \right] \frac{mon^O}{mon^S} \quad , \tag{1}$$

where

T_i = transmission in TOF channel i

C_i^S = dead-time–corrected counts for the sample measurement

TABLE I

Sample Thicknesses Used During the Carbon Experiment and Associated Number Densities Used in Analysis

Sample	Nominal Thickness (cm)	Diameter (cm)	Weight (g)	N (atom/b)
Graphite	7	7.499 ± 0.002	521.87 ± 0.01	0.5925 ± 0.0002
Graphite	13	7.498 ± 0.002	968.8 ± 0.1	1.1001 ± 0.0004
Graphite	33	7.496 ± 0.002	2469.3 ± 0.1	2.805 ± 0.001

TABLE II

Sample Thicknesses Used During the Beryllium Experiment and Associated Number Densities Used in Analysis

Sample	Nominal Thickness (cm)	Diameter (cm)	Weight (g)	N (atom/b)
Beryllium	2	7.498 ± 0.002	163.08 ± 0.01	0.24684 ± 0.00009
Beryllium	4	7.503 ± 0.002	326.60 ± 0.01	0.4937 ± 0.0002
Beryllium	8	7.501 ± 0.002	653.10 ± 0.01	0.9880 ± 0.0004
Graphite	13	7.498 ± 0.002	968.8 ± 0.1	1.1001 ± 0.0004

B_i^S = background counts for the sample measurement

C_i^O = dead-time–corrected counts for the open beam measurement

B_i^O = background counts for the open beam measurement

mon^O = monitor counts for the open beam measurement

mon^S = monitor counts for the sample measurement.

Since the background measurements B_i^S and B_i^O are derived from the dead-time–corrected data C_i^S and C_i^O, the same monitor correction is applied to both terms as shown in Eq. (1). Using the transmission data, we then obtain the total cross section using Eq. (2) for each TOF channel i:

$$\sigma_i = -\frac{1}{N}\ln(T_i) \quad , \tag{2}$$

where

σ_i = experimental total cross section in the TOF channel i

T_i = transmission in the TOF channel i

N = atomic number density of the sample (atom/b).

Two components contribute to the background shown in Eq. (1). The first component is room background, which is time independent and can be easily determined by collecting data with the LINAC off. The second component is associated with the production and transport of the pulsed neutron beam and varies with time. The time-dependent portion of the background is more difficult to obtain since it only occurs during operation and is therefore masked by the neutron spectrum. A typical technique that is used to measure the time-dependent background utilizes a resonance "notch" method,[10] in which materials are placed in the neutron beam that have black resonance regions in which a negligible number of neutrons are transmitted. Since few primary neutrons, those that are associated with the undisturbed collimated neutron beam, reach the detector, the counts in those resonances can be assumed to be background. However, the energy range of interest in this paper lacks materials with suitable resonances, which prohibits the use of this method. A new method has been developed to account for this time-dependent portion of the background.

Looking at a typical TOF spectrum, shown in Fig. 3, one can see that prior to the arrival of the gamma flash and subsequent neutrons, the counted data are at the room background level. This value has been shown to agree with a separately measured value with the LINAC off. Surrounding the gamma flash a buildup and decay of X-ray background can be seen. The X-ray background is a result of the detector picking up radiation emitted from the klystron radio-frequency amplifiers used to drive the

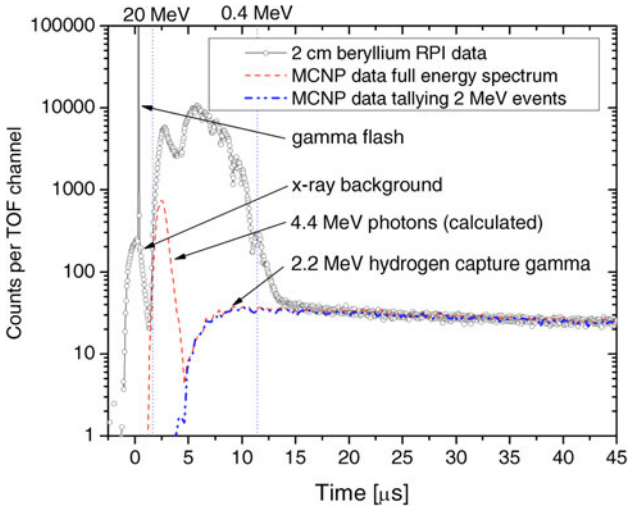

Fig. 3. A 2-cm beryllium MCNP calculation normalized to room background–subtracted experimental data. The full-energy-spectrum MCNP data show the combination of 2.2-MeV hydrogen capture photons and 4.4-MeV photons from the inelastic scattering of carbon in the scintillation medium and lead shielding surrounding the detector while the 2.2-MeV MCNP data show only photons tallied at that energy.

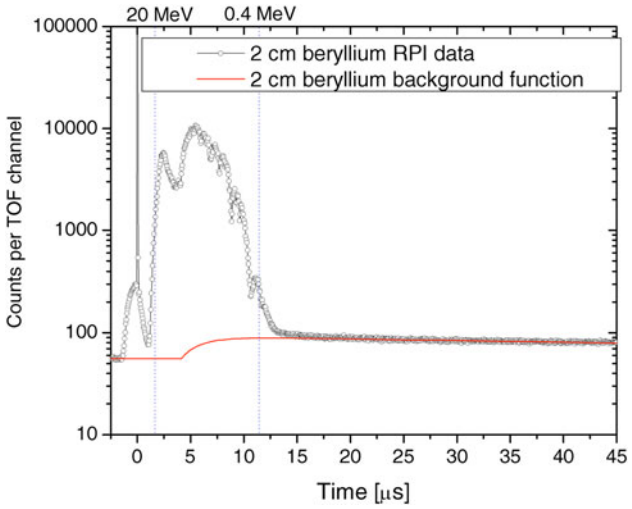

Fig. 4. The 2-cm beryllium experimental data and the calculated background function showing a good fit with the room background region (prior to gamma flash) and after primary neutron interaction (>20 μs).

accelerator. These X-rays are generated outside the target room and are atmospherically reflected (i.e., skyshine) before interacting with the detector. Lead shielding, 3.18 mm thick, was placed around the detector and klystrons to minimize this effect and to ensure that the X-rays are below a detectable level prior to neutron interaction. The addition of this shielding decreased the X-ray background by ~90%, and testing showed that with the shielding the X-rays are negligible at the 20-MeV TOF.

During the time primary neutrons are striking the detector, a time-dependent portion of the background builds and proceeds to decay back to room background at a long TOF (~1 ms). The cause of this time-dependent behavior was determined to be the thermalization of neutrons within the detector volume and the subsequent hydrogen capture accompanied by the release of a 2.2-MeV photon. Monte Carlo simulations were done using MCNP5 (Ref. 7), modeling the experimental setup from target to detector. Figure 4 shows the MCNP results normalized to room background–subtracted experimental data at long TOF (>20 μs). Two distinct photon energies can be distinguished in the MCNP analysis, 2.2-MeV hydrogen capture photons as well as 4.4-MeV photons from the inelastic scattering of neutrons with carbon atoms in the liquid scintillator medium. The photons from inelastic scattering occur nearly instantaneously and therefore can be considered an indication of a valid neutron interaction, effectively increasing the detector efficiency above 4.4 MeV.

The 2.2-MeV photons were tallied within the detector volume, and the exponential decrease seen in the calculation was fit to that seen in the experimental data, shown in Fig. 4. For ease in calculation the Monte Carlo background spectrum was fit to an analytical function using a least-squares–fitting algorithm. This time-dependent background is calculated for each sample condition and applied to Eq. (1) to determine the sample transmission.

Carbon (graphite) was chosen as a measurement reference because of the large amount of experimental data

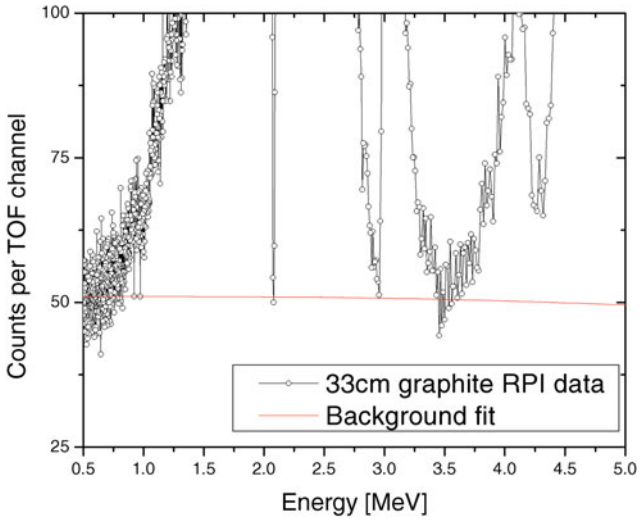

Fig. 5. Background calculation compared to thick (33-cm) graphite sample for background method verification. Background fit agrees within 8% to the "zero" transmission regions of the graphite sample.

as well as the consistency of the commonly used cross-section evaluations. Carbon also provides narrow resonance structure in the energy range of interest, which can be used to assess the resolution of the detection system. The measurement of carbon was taken during the beryllium experiment to be used as a benchmark.

The background method was verified by measuring a 33-cm graphite sample, shown in Fig. 5. At this graphite thickness there are several energy regions (0.5, 2.1, 2.9, and 3.5 MeV) with very low transmission (<0.001). In these regions it can be assumed the counts are from background alone, since 99.9% of the neutrons are removed from the beam. While this sample does contain black regions as required by the resonance notch method described above, the generally low neutron transmission through the sample over the energy range of interest prevents its use for that method. The difference in the integrated counts for each of these regions from the calculated background deviates by a maximum of 8%.

V. DATA ANALYSIS

Data were collected for the sample and open beam measurements into approximately 400 individual files, each file designated as a single sample run. These files were dead-time corrected and summed using the RPIXDR code.[11] The data were also checked for consistency using the MONCHK analysis code.[12] MONCHK was written to perform statistical checks on the data runs and reports any abnormalities for further examination. MONCHK also indicates which neutron beam monitor is best correlated with the EJ-301 detector to be used for data analysis. The selected monitor is used to normalize the data to account for variations in the neutron beam intensity over time. These slight variations over time are also the reason each sample run is kept short (~20 min), repeating each sample approximately once per hour.

The transmission for each sample was calculated using Eq. (1). The uncertainty in the transmission, Eq. (3), was determined by propagating the individual uncertainties in Eq. (1), assuming that the associated uncertainties are not correlated:

$$\frac{\Delta T}{T} = \sqrt{\left(\frac{\Delta C^s}{C^s - B^s}\right)^2 + \left(\frac{\Delta C^o}{C^o - B^o}\right)^2 + \left(\frac{\Delta B^s}{C^s - B^s}\right)^2 + \left(\frac{\Delta B^o}{C^o - B^o}\right)^2 + \left(\frac{\Delta mon^s}{mon^2}\right)^2 + \left(\frac{\Delta mon^o}{mon^o}\right)^2} \quad , \tag{3}$$

where

ΔC^s = statistical uncertainty in the sample counts C^s

ΔC^o = statistical uncertainty in the open beam counts C^o

ΔB^s = uncertainty in the sample background counts B^s

ΔB^o = uncertainty in the open beam background counts B^o

Δmon^s = statistical uncertainty in the monitor data taken during the sample measurement mon^s

Δmon^o = statistical uncertainty in the monitor data taken during the open measurement mon^o.

The statistical uncertainties used in Eq. (3) are taken from the 1σ counting statistics of the data collected in the individual time bins. The uncertainty in the background counts was estimated by doing a sensitivity study, varying the background count rates, and looking at the effect on the carbon data. It was shown that the background can be varied by 8% resulting in a <1% change in the transmission throughout most of the measured energy range.

The total cross section was calculated from the transmission using Eq. (2). The uncertainty in the cross section $\Delta\sigma$ for each channel bin was calculated using Eq. (4):

$$\Delta\sigma = \frac{1}{N}\frac{\Delta T}{T} \quad . \tag{4}$$

The uncertainty in the number density N is very small compared to the uncertainty in the transmission and is therefore neglected.

To combine the total cross-section values obtained for the n independent sample thicknesses measured, we used the weighted average of the measurements as shown in Eq. (5):

$$\bar{\sigma} = \frac{\sum_{i=1}^{n} \frac{\sigma_i}{(\Delta\sigma_i)^2}}{\sum_{i=1}^{n} \frac{1}{(\Delta\sigma_i)^2}} \quad . \tag{5}$$

The method for determining the uncertainty in the weighted average was adopted from the method used by Danon et al.[9] In this method two uncertainty sources are considered. The first source is the uncertainty resulting from the individual measurement uncertainties, which

we call the internal uncertainty. The internal uncertainty in the weighted average cross-section value is given in Eq. (6):

$$\Delta\sigma_{internal} = \left(\sum_{i=1}^{n} \frac{1}{(\Delta\sigma_i)^2} \right)^{-1/2} . \quad (6)$$

The second source of uncertainty is taken from the deviation in the total cross-section values between the individual sample thicknesses measured. This source is termed the external uncertainty and is expressed using Eq. (7):

$$\Delta\sigma_{external} = \sqrt{\frac{\sum_{i=1}^{n} \frac{(\bar{\sigma} - \sigma_i)^2}{(\Delta\sigma_i)^2}}{(n-1)\sum_{i=1}^{n} \frac{1}{(\Delta\sigma_i)^2}}} . \quad (7)$$

The uncertainty in the weighted average total cross section is then conservatively taken to be the maximum value obtained from the internal and external uncertainties [Eq. (8)]:

$$\Delta\bar{\sigma} = \max(\Delta\sigma_{internal}, \Delta\sigma_{external}) . \quad (8)$$

The energy for each TOF channel i was determined using the time stamp on the channel and the distance from neutron source to detector. The time of neutron emission, time zero t_0, can be determined using the gamma rays produced during the neutron production process in the target, the gamma flash, which can be directly measured with the detector array. The flight time of these photons is then used to back out the time zero allowing the flight time and velocity of the neutrons to be determined. With energies of interest in this measurement up to 20 MeV, the relativistic formula was used for accurate energy conversion as shown by Eq. (9):

$$E_i = m_o c^2 \left[\frac{1}{\sqrt{1 - \frac{L^2}{t_i^2 c^2}}} - 1 \right] , \quad (9)$$

where

$m_o c^2$ = rest mass energy of a neutron

t_i = neutron TOF at channel i

L = flight path distance.

The magnitude of the uncertainty in the energy corresponding to TOF channel i can be determined using Eq. (10):

$$|\Delta E| = \sqrt{\left(\frac{\partial E}{\partial t_i}\Delta\tau_p\right)^2 + \left(\frac{\partial E}{\partial t_i}\Delta\tau_c\right)^2 + \left(\frac{\partial E}{\partial L}\Delta L_T\right)^2 + \left(\frac{\partial E}{\partial L}\Delta L_D\right)^2} , \quad (10)$$

where

$\Delta\tau_p$ = uncertainty in the TOF due to the pulse width of the neutrons exiting the neutron target

$\Delta\tau_c$ = uncertainty in the TOF due to the channel width

ΔL_T = uncertainty in L due to the thickness of the neutron-producing target

L = flight path distance from the neutron source to the detector

ΔL_D = uncertainty in L due to the thickness of the detector.

VI. RESULTS

Figure 6 shows the present neutron total cross section for carbon compared to other experimental measurements,[9,13–16] selected from the greater than 30 reported measurements done on carbon in this energy range for their low cross-section uncertainty. There is very little difference in cross-section value between the current RPI measurement and those reported, as seen in Fig. 6. The present carbon cross section is also in excellent agreement with the commonly used evaluations, shown in Fig. 7. These results were used to validate the experimental system and the analytic procedures used to determine the neutron total cross section. The excellent agreement provides this validation.

The beryllium total cross section from this measurement is in good agreement with several prior measurements[9,17–20] selected for their low uncertainty, shown in Fig. 8. The measurements all agree above ~1.5 MeV while showing some deviation in the 0.4- to 1.5-MeV energy range. Figure 9 compares commonly used evaluations for beryllium neutron total cross section[6,21–23] in the energy range 0.4 to 20 MeV. The evaluations generally show good agreement with the exception of 0.4 to 1.5 MeV and 5.5 to 8.0 MeV, where some deviation can be seen. A difference of ~8% can be seen in the evaluations below 0.6 MeV and 5% between 5.5 and 8.0 MeV.

The present beryllium measurement shows a generally good agreement with the total cross-section evaluations over the measured energy range with some notable exceptions. From 400 to 600 keV the measured data follow JENDL 4.0 and are within a few percent of ENDF/B-VI.8 and JEFF 3.1 while ENDF/B-VII.0 is low by ~8%. The 621-keV resonance is shown to agree with ENDF/B-VI.8, ENDF/B-VII.0, and JEFF 3.1, while it is shifted ~2% low in JENDL 4.0. From 700 to 800 keV

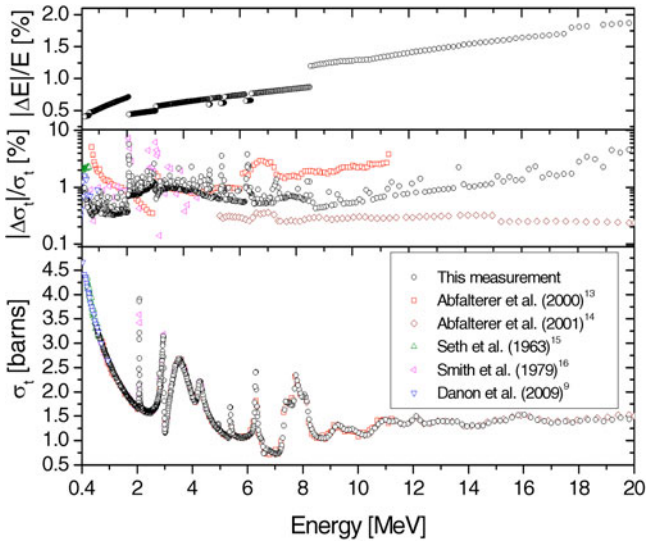

Fig. 6. Carbon data compared with other experimental cross-section data taken from EXFOR (bottom) with the relative uncertainties (middle) and fractional uncertainty in measured energy (top). Sudden deviation in uncertainty represents where TOF compression points were used. The measurements from EXFOR were selected based on the lowest uncertainty throughout the energy range of interest.

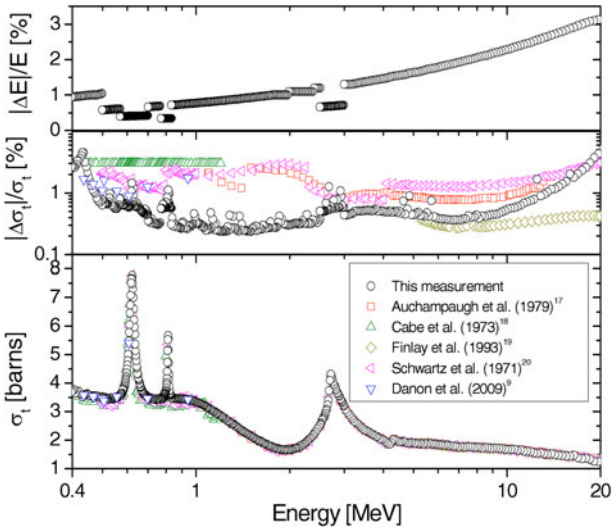

Fig. 8. Beryllium measurement compared with other experimental cross-section data taken from EXFOR (bottom) with the relative uncertainties (middle) and fractional uncertainty in measured energy (top). Sudden deviation in uncertainty represents where TOF compression points were used. The measurements from EXFOR were selected based on the lowest uncertainty throughout the energy range of interest.

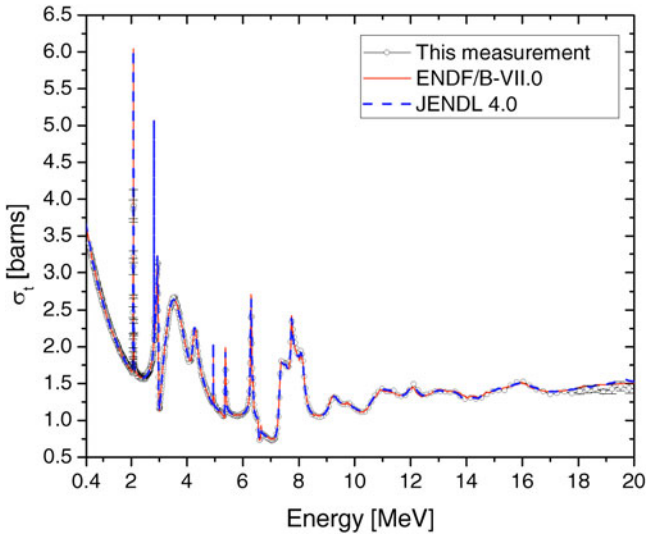

Fig. 7. Neutron total cross-section results for carbon compared to commonly used cross-section evaluations. ENDF/B-VI.8 and JEFF 3.1 are identical to ENDF/B-VII.0. If not shown, the measurement uncertainty is within the diameter of the point.

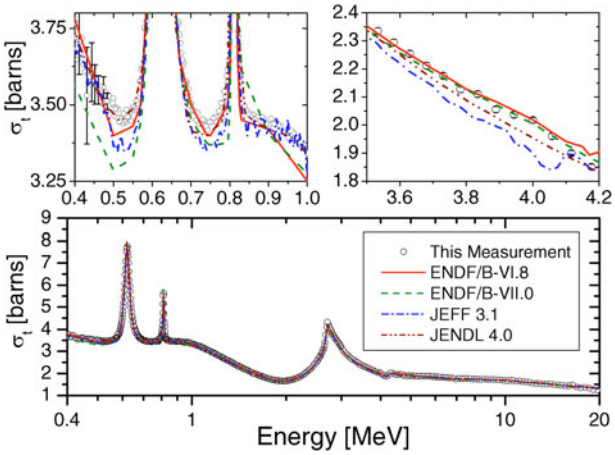

Fig. 9. Beryllium neutron total cross-section results compared to commonly used evaluations for the energy ranges 0.4 to 1 MeV (top left), 3.5 to 4.2 MeV (top right), and 0.4 to 20 MeV (bottom). The measured data are in best agreement with the ENDF/B-VI.8 evaluation through most of the measured energy range. ENDF/B-VII.0 is shown to be below the measured data in the range 0.4 to 0.55 MeV. For energies greater than 0.5 MeV, the measurement uncertainty is within the diameter of the point shown.

the measured data follow ENDF/B-VI.8 while ENDF/B-VII.0 and JEFF 3.1 trend ~2% low. In the energy range 3.5 to 4.1 MeV, the measured data follow ENDF/B-VI.8 and ENDF/B-VII.0 while JENDL 4.0 tracks ~1% low, and JEFF 3.1 tracks ~5% low. In the energy range from 5.5 to 8.0 MeV, the present measurement tracks JEFF 3.1 and JENDL 4.0 while ENDF/B-VI.8 and ENDF/B-VII.0 are ~2% lower.

The present measurement is also shown to be in excellent agreement with the high-accuracy measurement

done on beryllium by Danon et al.[9] at low energies and Finlay et al.[19] at high energies. Since the original writing of this paper, ENDF/B-VII.1 (Ref. 24) was released, which used the Danon et al. data to update the beryllium evaluation. The beryllium data in this evaluation show closer agreement to the presented data than the previous release, ENDF/B-VII.0.

VII. CONCLUSIONS

This paper presents a new detector system deployed at the Gaerttner LINAC Laboratory at RPI and new measurements of carbon and beryllium neutron total cross section in the energy range 0.4 to 20 MeV. The major component of the system's time-dependent background was determined to be 2.2-MeV photons from thermal neutron capture within the detector volume. This background component was simulated using MCNP5 and verified to within 8% using a thick carbon sample. The 8% uncertainty in simulated background typically contributes $<1\%$ to the overall cross-section uncertainty.

Measurements of the well-known carbon cross section are in excellent agreement throughout the energy range of interest. Measurements of the beryllium cross section are in general agreement with all the evaluations through most of the measured energy range. Below $\sim$1 MeV the JENDL 4.0 evaluation uses the RPI data from Ref. 9, which are also in excellent agreement with the present data. In the 700- to 800-keV and 3.5- to 4.1-MeV regions, the present data are in good agreement with the ENDF/B-VI.8 and ENDF/B-VII.0 cross sections, while those provided by JEFF 3.1 and JENDL 4.0 show some deviation. From 5.5 to 8.0 MeV the current beryllium measurement is in agreement with the JEFF 3.1 and JENDL 4.0 evaluated cross sections, where ENDF/B-VI.8 and ENDF/B-VII.0 are $\sim$2% low. Additionally, the 621-keV resonance energy in the present data agrees with ENDF/B-VI.8, ENDF/B-VII.0, and JEFF 3.1, where the JENDL 4.0 energy is $\sim$2% low.

This new measurement can help resolve the issues seen in the beryllium evaluations in the noted energy ranges by providing high-resolution, high-accuracy data. The quality of this beryllium measurement can additionally reduce the uncertainty in the beryllium total neutron cross-section evaluations in the energy range of 0.4 to 20 MeV.

ACKNOWLEDGMENTS

The authors would like to thank the RPI LINAC operators and staff P. Brand, M. Grey, M. Strock, and A. Kerdoun for their technical expertise and work in running the LINAC during the experiments.

REFERENCES

1. T. A. TOMBERLIN, "Beryllium—A Unique Material in Nuclear Applications," *Proc. 36th Int. SAMPE Technical Conf.*, San Diego, California, November 15–18, 2004, Society for the Advancement of Material and Process Engineering (2004).

2. M. C. BILLONE, M. DALLE DONNE, and R. G. MACAULAY-NEWCOMBE, "Status of Beryllium Development for Fusion Applications," *Proc. Third Int. Symp. Fusion Nuclear Technology*, Los Angeles, California, June 26–July 1, 1994.

3. "EXFOR Systems Manual: Nuclear Reaction Data Exchange Format," BNL-NCS-63330, V. McLANE, Ed., Nuclear Data Centers Network, National Nuclear Data Center, Brookhaven National Laboratory (1996).

4. M. E. OVERBERG et al., "Photoneutron Target Development for the RPI Linear Accelerator," *Nucl. Instrum. Methods Phys. Res., Sect. A*, **438**, 253 (1999).

5. F. SAGLIME, PhD Thesis, Rensselaer Polytechnic Institute (2009).

6. M. B. CHADWICK et al., "ENDF/B-VII.0: Next Generation Evaluated Nuclear Data Library for Nuclear Science and Technology," *Nucl. Data Sheets*, **107**, 2931 (2006).

7. X-5 MONTE CARLO TEAM, "Computer Code MCNP—A General Monte Carlo N-Particle Transport Code, Version 5," LA-UR-03-1987, Los Alamos National Laboratory (2003).

8. Y. DANON and R. C. BLOCK, "Minimizing the Statistical Error of Resonance Parameters and Cross Sections Derived from Transmission Measurements," *Nucl. Instrum. Methods*, **485**, 585 (2002).

9. Y. DANON et al., "Beryllium and Graphite High-Accuracy Total Cross-Section Measurements in the Energy Range from 24 to 900 keV," *Nucl. Sci. Eng*., **161**, 321 (2009).

10. D. B. SYME, "The Black and White-Filter Method for Background Determination in Neutron Time-of-Flight Spectrometry," *Nucl. Instrum. Methods*, **198**, 357 (1982).

11. Y. DANON, "Rensselaer Polytechnic Institute Cross Section Data Reduction Computer Code (RPIXDR1.10.1)," Rensselaer Polytechnic Institute (2006).

12. Y. DANON, PhD Thesis, Rensselaer Polytechnic Institute (1993).

13. W. P. ABFALTERER, R. W. FINLAY, and S. M. GRIMES, "Level Widths and Level Densities of Nuclei in the $32 \leq A \leq 60$ Mass Region Inferred from Fluctuation Analysis of the Total Cross Section," *Phys. Rev. C: Nucl. Phys*., **62**, 064312 (2000).

14. W. P. ABFALTERER et al., "Measurement of Neutron Total Cross Sections up to 560 MeV," *Phys. Rev. C: Nucl. Phys*., **63**, 044608 (2001).

15. K. K. SETH, E. G. BILPUCH, and H. W. NEWSON, "Total Neutron Cross Section of Carbon," *Nucl. Phys*., **47**, 137 (1963).

16. A. SMITH, R. HOLT, and J. WHALEN, "Neutron Interaction with Carbon-12 in the Few-MeV Region," *Nucl. Sci. Eng*., **70**, 281 (1979).

17. G. F. AUCHAMPAUGH, S. PLATTARD, and N. W. HILL, "Neutron Total Cross-Section Measurements of ^{9}Be, ^{10,11}B, and ^{12,13}C from 1.0 to 14 MeV Using the ^{9}Be-9$(d,n)^{10}$B Reaction as a 'White' Neutron Source," *Nucl. Sci. Eng*., **69**, 30 (1979).

18. J. CABE and M. CANCE, "Measurements of the Neutron Total Cross Sections of Be, B-11, C, Al, Si, S, Ti, V, Ni, U-235, U-238, Pu-239 Between 100 keV and 6 MeV," *C. R. Phys*., **258**, 1478 (1973); see also EXFOR entry 10070003: http://www.nndc.bnl.gov/exfor/exfor00.htm (current as of Aug. 10, 2011).

19. R. W. FINLAY et al., "Neutron Total Cross Sections at Intermediate Energies," *Phys. Rev. C: Nucl. Phys*., **47**, 237 (1993).

20. R. B. SCHWARTZ, R. A. SCHRACK and H. T. HEATON, "Total Neutron Cross Sections of Silicon and Beryllium," *Bull. Am. Phys. Soc*., **16**, 495 (1971).

21. CROSS SECTION EVALUATION WORKING GROUP, "ENDF-201, ENDF/B-VI Summary Documentation," BNL-NCS-17541, Brookhaven National Laboratory (1991).

22. A. KONING et al., "JEFF Report 21: The JEFF-3.1 Nuclear Data Library," Nuclear Energy Agency (2006).

23. K. SHIBATA et al., "JENDL-4.0: A New Library for Nuclear Science and Engineering," *J. Nucl. Sci. Technol*., **48**, 1 (2011).

24. M. B. CHADWICK et al., "ENDF/B-VII.1 Nuclear Data for Science and Technology: Cross Sections, Covariances, Fission Product Yields, and Decay Data," *Nucl. Data Sheets*, **112**, *12*, 2887 (2011).